Journal of Experimental Botany
doi:10.1093/jxb/erz442 Advance Access Publication 15 November 2019
This paper is available online free of all access charges (see https://academic.oup.com/jxb/pages/openaccess for further details)

RESEARCH PAPER

Photosynthetic efficiency and mesophyll conductance are unaffected in *Arabidopsis thaliana* aquaporin knock-out lines

Johannes Kromdijk[1,2,*], Katarzyna Głowacka[2,3,4] and Stephen P. Long[2,5]

[1] Department of Plant Sciences, University of Cambridge, Downing street, Cambridge CB2 3EA, UK
[2] Carl R. Woese Institute for Genomic Biology, University of Illinois at Urbana-Champaign, 1206 West Gregory drive, Urbana, IL 61801, USA
[3] Institute of Plant Genetics, Polish Academy of Sciences, 60-479 Poznań, Poland
[4] Department of Biochemistry, University of Nebraska-Lincoln, N246 Beadle Center, 1901 Vine Street, Lincoln, NE 68588-0664, USA
[5] Lancaster Environment Centre, University of Lancaster, Lancaster LA1 1YX, UK

* Correspondence: jk417@cam.ac.uk

Received 9 July 2019; Editorial decision 16 September 2019; Accepted 6 October 2019

Editor: Christine Raines, University of Essex

Abstract

Improving photosynthetic efficiency is widely regarded as a major route to achieving much-needed yield gains in crop plants. In plants with C_3 photosynthesis, increasing the diffusion conductance for CO_2 transfer from substomatal cavity to chloroplast stroma (g_m) could help to improve the efficiencies of CO_2 assimilation and photosynthetic water use in parallel. The diffusion pathway from substomatal cavity to chloroplast traverses cell wall, plasma membrane, cytosol, chloroplast envelope membranes, and chloroplast stroma. Specific membrane intrinsic proteins of the aquaporin family can facilitate CO_2 diffusion across membranes. Some of these aquaporins, such as PIP1;2 in *Arabidopsis thaliana*, have been suggested to exert control over g_m and the magnitude of the CO_2 assimilation flux, but the evidence for a direct physiological role of aquaporins in determining g_m is limited. Here, we estimated g_m with four different methods under a range of light intensities and CO_2 concentrations in two previously characterized *pip1;2* knock-out lines as well as *pip1;3* and *pip2;6* knock-out lines, which have not been previously evaluated for a role in g_m. This study presents the most in-depth analysis of g_m in Arabidopsis aquaporin knock-out mutants to date. Surprisingly, all methods failed to show any significant differences between the *pip1;2*, *pip1;3*, or *pip2;6* mutants and the Col-0 control.

Keywords: Aquaporin, CO_2 assimilation, mesophyll conductance, photosynthetic efficiency, PIP.

Introduction

Global agricultural food production may need to increase by 50% in 2050 to keep track of the predicted increase in the global human population and predicted dietary shifts (Tilman *et al.*, 2011; FAO, 2017). Marginal yield gains via traditional breeding strategies have recently started to decline for several major crops, emphasizing the need for new unexplored strategies with potential for yield improvement (Ray *et al.*, 2013). Importantly, achieving these vast increases in agricultural demand while meeting sustainability targets will require new strategies to intensify productivity per unit land area and per unit available water (Hunter *et al.*, 2017). Improving photosynthetic efficiency may hold untapped potential for

sustainable yield improvement (e.g. Long *et al.*, 2015; Ort *et al.*, 2015), as demonstrated by improvement of photosynthetic efficiency via free air CO_2 enrichment (Ainsworth and Long, 2005; Hasegawa *et al.*, 2013) as well as via transgenic alleviation of photosynthetic bottlenecks (Rosenthal *et al.*, 2011; Kromdijk *et al.*, 2016; Köhler *et al.*, 2017; South *et al.*, 2019) both of which lead to significant productivity increases under field conditions.

One strategy to improve the efficiency of photosynthesis is by increasing the availability of CO_2 in the chloroplast stroma. Increasing stromal [CO_2] helps to improve the efficiency of carbon fixation by ribulose bisphosphate carboxylase/oxygenase (Rubisco), by increasing substrate availability and by competitive inhibition of ribulose bisphosphate (RuBP) oxygenation. To get from the atmosphere into the chloroplast, CO_2 diffuses through the leaf boundary layer, stomatal pores, intercellular airspace, cell wall, plasma membrane, cytosol, chloroplast envelope membranes, and part of the chloroplast stroma. The conductance across the pathway from intercellular airspace to chloroplast stroma is termed mesophyll conductance or g_m. Increasing g_m has attracted a lot of interest, because of its potential to simultaneously improve photosynthetic efficiency and intrinsic water use efficiency (Flexas *et al.*, 2013*a*). g_m is partially determined by the CO_2 conductance through the plasmalemma and chloroplast envelope. If the diffusion resistance through these membranes represents a significant component of g_m, as model results suggest (Von Caemmerer and Evans, 2015), factors that facilitate CO_2 diffusion across membranes should correlate with g_m. Consistent with this suggestion are several reports of control of facilitated diffusion of CO_2 across membranes by specific aquaporins and concomitant stimulation of photosynthetic CO_2 fixation (e.g. Uehlein *et al.*, 2003; Flexas *et al.*, 2006; Heckwolf *et al.* 2011).

Aquaporins are membrane channel proteins that were initially identified and named based on their facilitating role in transmembrane water transport (Agre *et al.*, 1993; Maurel, 1997). Subsequent work has identified a wide variety of aquaporins, which can increase membrane permeability to specific small molecules such as urea (CH_4N_2O), glycerol ($C_3H_8O_3$), ammonia (NH_3), hydrogen peroxide (H_2O_2), and CO_2 (see reviews by Maurel *et al.* (2015) and Groszmann *et al.* (2017) and references therein). Although aquaporins aggregate into tetrameric structures, the monomeric protein is the functional unit and contains several conserved structural features. Each aquaporin monomer contains six membrane-spanning domains and five connecting loops. The membrane-spanning pore contains an aromatic/arginine configuration (Ar/R) at the centre, providing a selective filter where molecules can pass single-file. Additionally, the loop A and loop D α-helices carry asparagine–proline–alanine (NPA) motifs, which are positioned near the central narrow pore, which helps prevent permeability to protons and contributes to the selectivity of the channel (Bansal and Sankararamakrishnan, 2007). Reversible conformational change can move a hydrophobic residue on the cytoplasmic loop D into or out of the central opening (Tournaire-Roux *et al.*, 2003; Törnroth-Horsefield *et al.*, 2006), allowing the monomeric pore to be toggled in open or closed configuration. Cations, pH, and phosphorylation are among the factors that affect aquaporin activity (i.e. the fraction of open channels) and are typically associated with opening or closing of the monomeric pore. However, the hetero-tetrameric clustering creates an additional pore in between the four monomers that may also affect membrane permeability, but without the gating functionality (Otto *et al.*, 2010; Frick *et al.*, 2013). With regards to permeability to CO_2, an isoleucine to methionine mutation on the E-loop was shown to completely abolish CO_2 permeability in barley aquaporins (Mori *et al.*, 2014). The strong conservation of this sequence in most, if not all, CO_2 conducing aquaporins identified to date may indicate a general relevance of the E-loop conformation to facilitation of CO_2 permeability.

Whereas aquaporin-associated increases in CO_2 permeability were demonstrated in experimental membrane systems such as oocytes or yeast (e.g. Uehlein *et al.*, 2003; Otto *et al.*, 2010), the physiological relevance of these findings *in vivo* is not without contention and has been debated in the context of specific physiological roles in both the animal and plant kingdoms (e.g. Evans *et al.*, 2009; Endeward *et al.*, 2014). Experimental verification of a physiological role of aquaporin in g_m is complicated due to the lack of experimental procedures to directly assess g_m. Instead, g_m has to be derived by indirect methods, which are notoriously troublesome (e.g. Tholen *et al.*, 2012; Gu and Sun, 2014). Possibly as a result, evidence in experimental membrane systems is sometimes used to implicate control of specific aquaporins over g_m (Uehlein *et al.*, 2003), whereas data specifically linking manipulation of aquaporin expression to changes in g_m are often limited to a single set of conditions (e.g. Xu *et al.*, 2019).

In this context, we set out on a new and detailed attempt to assess whether lack of expression of specific aquaporins in Arabidopsis can be linked with variation in g_m and photosynthetic efficiency. To do so, we used Arabidopsis aquaporin T-DNA insertional mutants with four different methods of estimating g_m *in vivo* under various CO_2 concentrations and light intensities. This presents (to our knowledge) the most in-depth analysis of g_m in aquaporin knock-out mutants to date. In addition to assessing differences in g_m as a result of knocking out PIP1;2, which has been previously implicated to have a role in facilitating membrane CO_2 permeability *in vivo* (Heckwolf *et al.*, 2011; Uehlein *et al.*, 2012), we also included *pip1;3* and *pip2;6* mutants, deficient for two more aquaporin family members, which have not previously been evaluated for a role in mesophyll conductance. PIP1;3 is annotated to be both chloroplast and plasma membrane located (The Arabidopsis Information Resource), is expressed ubiquitously throughout development, and is very similar in sequence to PIP1;2 (87% similarity in amino acid sequence). PIP2;6 is primarily expressed in leaves at relatively high levels (Alexandersson *et al.*, 2005) and has been reported to show co-expression with genes involved in photosynthesis (Da Ines, 2008). Additionally, both PIP1;3 and PIP2;6 contain the isoleucine in the conserved E-loop sequence, which was required for CO_2 permeability in barley aquaporins (Mori *et al.*, 2014). Perhaps surprisingly, we demonstrate that none of the methods provided any evidence to suggest that g_m had been altered by the absence of PIP1:2, PIP1;3, or PIP2;6. Instead, g_m and photosynthetic efficiency in

pip1;2, *pip1;3*, and *pip2;6* plants were indistinguishable from the Col-0 control plants under a wide range of CO_2 concentrations and light intensities.

Materials and methods

Mutant verification

Arabidopsis seeds were obtained for T-DNA insertional mutant lines *pip1-2* (Salk019794C and Salk145347C), *pip1-3* (Salk051107C), *pip2-6* (Salk029718C) and Col-0 ecotype (CS28168) from the Arabidopsis Biological Resource Center at Ohio State University (Alonso *et al.*, 2003). After one round of selfing, positional T-DNA insertions and homozygosity were confirmed on the offspring using PCR reactions with the LBb1.3 primer (5′-ATTTTGCCGATTTCGGAAC-3′) on pROK2 in combination with sequence-specific primers flanking the reported insertion (designed using the primer design tool on http://signal.salk.edu/tdnaprimers.2.html; see Supplementary Table S1 at *JXB* online). To confirm that the T-DNA insertion led to complete lack of expression of mature transcript, mRNA was extracted from leaf discs (NucleoSpin RNA/Protein kit, REF740933, Macherey-Nagel GmbH & Co. KG, Düren, Germany), treated with DNase (Turbo DNA-free kit; AM1907, Thermo Fisher Scientific, Waltham, MA, USA) and transcribed to cDNA (Superscript III First-Strand Synthesis System for RT-PCR, 18080-051, Thermo-Fisher Scientific). Primers designed against the 5′ and 3′ untranslated region (UTR) (Supplementary Table S1) were used to test for the presence of mature transcripts in cDNA preparations. No mature transcript was detected in cDNA from *pip1-3* plants (Salk051107C) and *pip1-2* (Salk019794C and Salk145347C), but in the reaction of *pip2-6* (Salk029718C) a weak band was detected of the same size as in the Col-0 control. These residual *PIP2;6* mRNA levels in Salk029718C were quantified relative to Col-0 using RT-qPCR with primers spanning the T-DNA insertion (Supplementary Table S1) and normalized to amplicons in EF1α and UBQ10.

Plant propagation

Seeds were sown on moist filter paper in Petri dishes and stratified for 4 d at 4 °C. After germination, seeds were transferred to pots with a soil-less potting mix (LC1 Sunshine mix, Sun Gro Horticulture, Agawam, MA, USA) and positioned in a controlled-environment chamber (PGC20, Conviron, Winnipeg, Canada) with photoperiod set to 10 h and air temperature controlled at 18 °C/21 °C (night/day). Light intensity at leaf level was controlled at 200 µmol m^{-2} s^{-1}. Plants were watered and repositioned at random every 2 d, to avoid confounding individuals with any undetected environmental variation within the chamber. All gas exchange measurements were performed on fully expanded leaf 10, 11 or 12. Independent batches of plants were used for each experiment described.

Estimating g_m from carbon isotope discrimination ($\Delta^{13}C$) during photosynthetic gas exchange

Leaves were clamped in the cuvette of an open gas exchange system (LI6400XT, LI-COR, Lincoln, NE, USA) with 6 cm^2 integrated LED light source (6400-02B, LI-COR). When leaves did not fully fill the cuvette area, the leaf area inside the cuvette was photographed and measured using image processing software ImageJ (1.51S version 1.8.0_66, National Institutes of Health, USA). Light intensity was set to 500 µmol m^{-2} s^{-1}, block temperature controlled at 25 °C and CO_2 concentration in the airstream maintained at 400 µmol mol^{-1}. CO_2 from reference line air and exhaust air from the cuvette were purified using two parallel cryogenic trapping and purification lines under partial vacuum as described in Kromdijk *et al.* (2010). After net assimilation and stomatal conductance had reached steady state, two replicate samples of CO_2 were collected from each line for 5 min each, while gas exchange parameters were recorded simultaneously. Carbon isotope composition of collected CO_2 was analysed on an isotope ratio mass spectrometer (SIRA series II, VG Isotech, modified by Provac Ltd, Crewe, UK). Observed $\Delta^{13}C$ was derived from measured CO_2 mole fractions and isotope compositions in reference and cuvette air, according to Evans *et al.* (1986). Derivation of g_m from observed $\Delta^{13}C$ was done according to equations outlined in Evans and Von Caemmerer (2013), using 29‰ for Rubisco fractionation factor b and 16.2‰ for photorespiratory fractionation factor f. Estimations of g_m based on isotope discrimination as well as J-based methods (below) were normalized to air pressure using the LI6400XT pressure sensor. The CO_2 compensation point in the absence of dark respiration (Γ^*) for Arabidopsis was computed from measured leaf temperature according to Walker *et al.* (2013).

Estimating g_m using variable and constant J

Leaves were clamped in the cuvette of an open gas exchange system (LI6400XT, LI-COR) with 2 cm^2 integrated fluorometer (Leaf Chamber Fluorometer, LI6400-40, LI-COR). Block temperature was controlled at 25 °C and CO_2 concentration in the airstream maintained at 400 µmol mol^{-1}. Leaves were equilibrated inside the cuvette until net CO_2 assimilation (A_n), stomatal conductance (g_s) and steady state fluorescence (F') were constant. Subsequently, gas exchange parameters were recorded and maximal fluorescence (F_m') was estimated using the multi-phase flash protocol (Loriaux *et al.*, 2013). Operating efficiency of photosystem II (Φ_{PSII}) was estimated using Eq. 1, following Genty *et al.* (1989):

$$\Phi_{PSII} = (F_m' - F') / F_m' \quad (1)$$

Leaf absorptance was estimated on the same spot where gas exchange measurements had been performed, using an integrating sphere (LI1800, LI-COR) connected with an optical fibre to a spectrometer with VIS-NIR grating (USB-2000, Ocean Optics Inc., Dunedin, FL, USA). Absorbed irradiance (I_{abs}) was computed by multiplying the incident irradiance with the measured absorptance at the emission wavelengths of the light source (470 and 630 nm). Measurements of chlorophyll fluorescence were used to estimate whole-chain electron transport rate (J) according to Eq. 2:

$$J = I_{abs} \times \Phi_{PSII} \times f_{PSII} \quad (2)$$

Here, f_{PSII} represents the relative absorption by photosystem II, which was taken as 0.5. Parallel measurements of photosynthetic gas exchange and J were used to derive g_m in two different ways. Measurements at various CO_2 concentrations (75, 100, 200, 300, 400, 600, 800, 1000, 1500 µmol mol^{-1}) performed at three light intensities (200, 500, and 1000 µmol m^{-2} s^{-1}) were used to estimate g_m according to the constant J method (Harley *et al.*, 1992). This method assumes that at moderately high CO_2 concentrations, Φ_{PSII} (and thus estimated J) will become constant. This assumption was justified for six measurements at light intensity of 200 µmol m^{-2} s^{-1} (coefficient of variation <3%), and for four measurements per light intensity at 500 and 1000 µmol m^{-2} s^{-1} (coefficient of variation <2%). These measurements were used in Eq. 3, where g_m was iteratively derived by minimizing the variance of J for each light intensity.

$$J = (A_n + R_l)\frac{s\left(\left(C_i - \frac{A_n}{g_m}\right) + 2\Gamma^*\right)}{\left(C_i - \frac{A_n}{g_m}\right) - \Gamma^*} \quad (3)$$

Measurements at varying CO_2 concentrations (400, 300, 250, 200, 150, 100, 75 µmol mol^{-1}) and constant light intensity (1000 µmol m^{-2} s^{-1}) or varying light intensity (50, 80, 110, 140, 170, 200, 300, 400, 500, 600, 700, 800, 1000 µmol m^{-2} s^{-1}) at constant CO_2 (400 µmol mol^{-1}) were used to estimate g_m using the variable J method (Harley *et al.*, 1992). In this method, the chloroplastic CO_2 concentration (C_c) is derived by matching gross CO_2 uptake with J, according to the following relationship:

$$C_c = \frac{\Gamma^*(J + 2s(A_n + R_l))}{(J - s(A_n + R_l))} \quad (4)$$

In both J-based methods, R_l represents mitochondrial respiration not associated with photorespiration under illuminated conditions, which was

estimated as 0.5 times the dark respiration rate R_d. Parameter s was estimated from the inverse of the slope of A_n as a function of J under 2% O_2 and 1500 μmol mol^{-1} CO_2 for each leaf. The estimate of C_c from Eq. 4 was used to derive g_m according to Fick's law:

$$g_m = A_n / (C_i - C_c) \quad (5)$$

*Inferring differences in g_m from the CO_2 compensation point C_i**

Leaves were clamped in the cuvette of an open gas exchange system (LI6400XT, LI-COR) with 6 cm^2 integrated LED light source (6400-02B, LI-COR). If leaf area inside the cuvette was less than 6 cm^2, it was accounted for as described above. The instrument plumbing was modified to control for low CO_2 concentrations in the airstream (LI-COR Application Note 7, https://www.licor.com/documents/iv8ljrga3fjsqc4nrhti.pdf). Block temperature was controlled at 25 °C. Leaves were equilibrated at light intensity of 200 μmol m^{-2} s^{-1} and CO_2 concentration was set at 400 μmol mol^{-1}. After net assimilation and stomatal conductance had reached steady state, CO_2 concentration was changed to 110, 90, 70, 50 and 30 μmol mol^{-1}. At each concentration, readings were logged when net assimilation rate had reached steady state. After the gas exchange parameters at 30 μmol mol^{-1} CO_2 were logged, CO_2 concentration was returned to 400 μmol mol^{-1} and net assimilation rate was allowed to recover for at least 15 min. Subsequently, the same measurement routine was repeated at light intensity of 170, 110, 75, and 50 μmol m^{-2} s^{-1}, providing a total of 25 observations per leaf (five CO_2 concentrations × five light intensities). Derivation of C_i* was performed using the slope–intercept method as described in Walker and Ort (2015). In short, measurements of net assimilation rate were plotted as a function of intercellular CO_2 concentration C_i. This resulted in five linear responses per leaf, which were all fitted to the general function:

$$A_n = mC_i + \gamma_0 \quad (6)$$

The resulting set of five (m, γ_0) pairs were subjected to linear regression, where the negative slope of the regression between m and γ_0 provided an estimate of C_i*. The CO_2 compensation point based on chloroplastic CO_2 (Γ*) is primarily determined by Rubisco kinetics and should therefore be equal between mutants and control. However, this is not the case for C_i* which should equal $\Gamma^* - (R_l/g_m)$, and hence potential differences in g_m between mutants and control should be reflected in C_i*.

Photosynthetic efficiency and capacity

Initial slopes of light response curves were determined to compare the maximum quantum yield of net assimilation rate A_n and J. A non-rectangular hyperbolic model was used to estimate the light-saturated rate of net assimilation rate A_{sat} and whole-chain electron transport J_{max}. The response curves of A_n to chloroplastic CO_2 concentration were used to derive $V_{c,max}$ by fitting a biochemical model of leaf photosynthesis (Von Caemmerer, 2000) to observations using temperature corrections from Walker *et al.*, (2013).

Statistical analysis

All statistical procedures were performed using SAS (v9.3, SAS Institute Inc., Cary, NC, USA). Data was tested for normality using the Kolgomorov–Smirnov test and homogeneity of variance using the Brown–Forsythe test. If either test discarded the null hypothesis, data were transformed or the Wilcoxon non-parametric test was applied. One-way analysis of variance was applied to g_m based on $\Delta^{13}C$, C_i*, $V_{c,max}$, and J_{max}. Repeated measures two-way analysis of variance was applied on g_m estimated with the constant J method at three light intensities. To compare g_m between mutant lines and Col-0 across various CO_2 concentrations and light intensities in the variable J experiment, 95% confidence intervals around mean g_m were generated for each condition, using the bias-corrected percentile method on a bootstrap of 1000 samples (*bootci* function in Matlab R2013a, The MathWorks Inc., Natick, MA, USA).

Results

Confirmation of molecular phenotype

The genomic structure around the T-DNA insertion and homozygosity were confirmed for each *pip* mutant lines (see Supplementary Fig. S1A). Primers amplifying the full mature transcript from 5′UTR to 3′UTR were used on cDNA preparations. No amplification of *PIP1;3* and *PIP1;2* transcript was detectable in cDNA preparations from the *pip1;3* (Salk051107C) and the two *pip1;2* mutant lines (Salk019794C and Salk145347C) (Supplementary Fig. S1B). However, the reactions with cDNA from the *pip2;6* mutant line (Salk029718C) showed weakly amplified fragments for *PIP2;6*, some of which matched the size of the amplicon in the Col-0 control (Supplementary Fig. S1B, lanes 2 and 3). Primers spanning the T-DNA insertion were used to quantify residual expression of mature *PIP2;6* mRNA in Salk029718C using RT-qPCR. The detectable cycle number normalized to *EF1α* and *UBQ10* was significantly higher for Salk029718C (12.96±0.39) compared with Col-0 (0.73±0.16). Based on these measurements, *PIP2;6* transcript was present in Salk029718C at 0.02% of the Col-0 expression levels (Supplementary Fig. S1C).

g_m estimated from $\Delta^{13}C$

g_m cannot be measured directly, but a number of methods exist to indirectly estimate it. Firstly, carbon isotope discrimination ($\Delta^{13}C$) measured in conjunction with photosynthetic gas exchange was used to estimate g_m. The ratio between C_i and CO_2 concentration in the air surrounding the leaf (C_a), i.e. the balance between diffusional and biochemical limitations during the measurements, was comparable between genotypes (Fig. 1A). $\Delta^{13}C$ averaged 19.3±0.4‰ across measurements and did not vary significantly between genotypes (Fig. 1B, P=0.86). Estimates of g_m based on these measurements ranged between 0.19 and 0.24 mol m^{-2} s^{-1} bar^{-1} and did not show any evidence of significant genotype effects on g_m (Fig. 1C, P=0.96).

g_m estimated from constant J

Parallel measurement of A_n and J at ambient or supra-ambient CO_2 concentrations were used to compute g_m using constant J. This method assumes that J becomes constant when electron transport is not inhibited by insufficient supply of CO_2. Measurements of Φ_{PSII} were used to make sure that this assumption was supported. Points selected for the constant J calculation varied less than 3% (coefficient of variation) for measurements at 200 μmol m^{-2} s^{-1} PFD and less than 2% for measurements at 500 and 1000 μmol m^{-2} s^{-1}. g_m estimated by constant J was somewhat lower than estimations using $\Delta^{13}C$ at the same light intensity of 500 μmol m^{-2} s^{-1} (0.07 versus 0.22 mol m^{-2} s^{-1} bar^{-1}). Analysis of variance showed a significant effect of light intensity on g_m estimated by constant J (P<0.0001), with average g_m decreasing by 26% at 500 μmol m^{-2} s^{-1} (Fig. 2B) and 51% at 200 μmol m^{-2} s^{-1} (Fig. 2A), relative to g_m at 1000 μmol m^{-2} s^{-1} (0.12 mol m^{-2} s^{-1} bar^{-1}, Fig. 2C). Analysis of variance showed no significant effect of genotype (P=0.69), consistent with g_m estimates based on $\Delta^{13}C$.

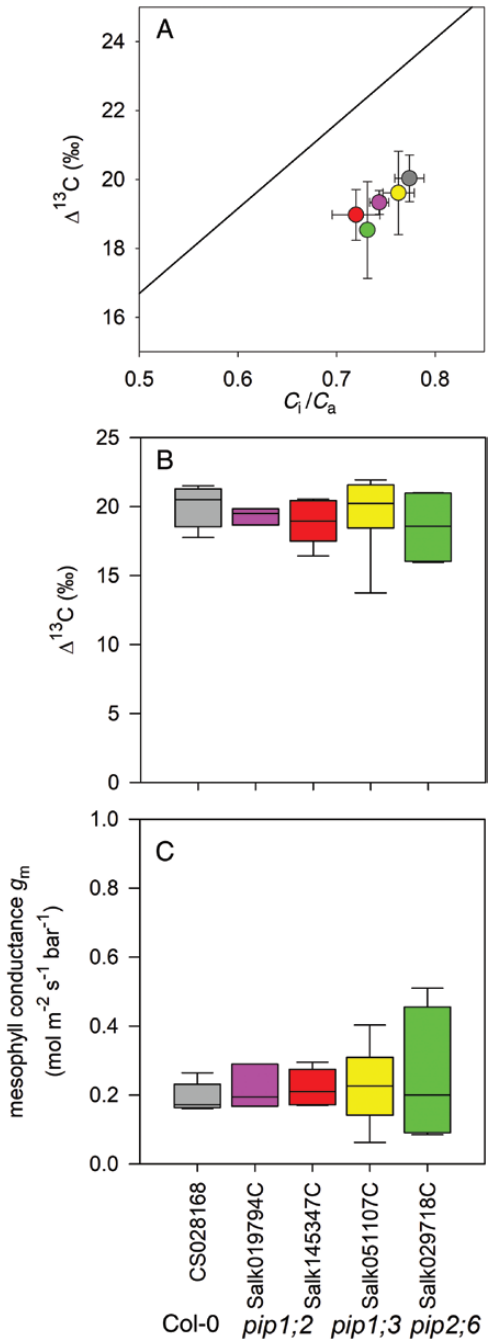

Fig. 1. Mesophyll conductance estimated from carbon isotope discrimination concurrently with photosynthetic CO_2 assimilation. (A) Isotope discrimination ($\Delta^{13}C$) as a function of C_i/C_a. Solid line shows theoretical isotope discrimination where $g_m=\infty$. Symbol colours correspond to different genotypes (grey: CS28168 (Col-0); pink: Salk019794C (*pip1;2*); red: Salk145347C (*pip1;2*); yellow: Salk051107C (*pip1;3*); green: Salk029718C (*pip2;6*)). Symbols show means ±SE (n=3–6). (B) Boxplots for isotope discrimination ($\Delta^{13}C$) per genotype. (C) Boxplots for mesophyll conductance g_m computed from $\Delta^{13}C$.

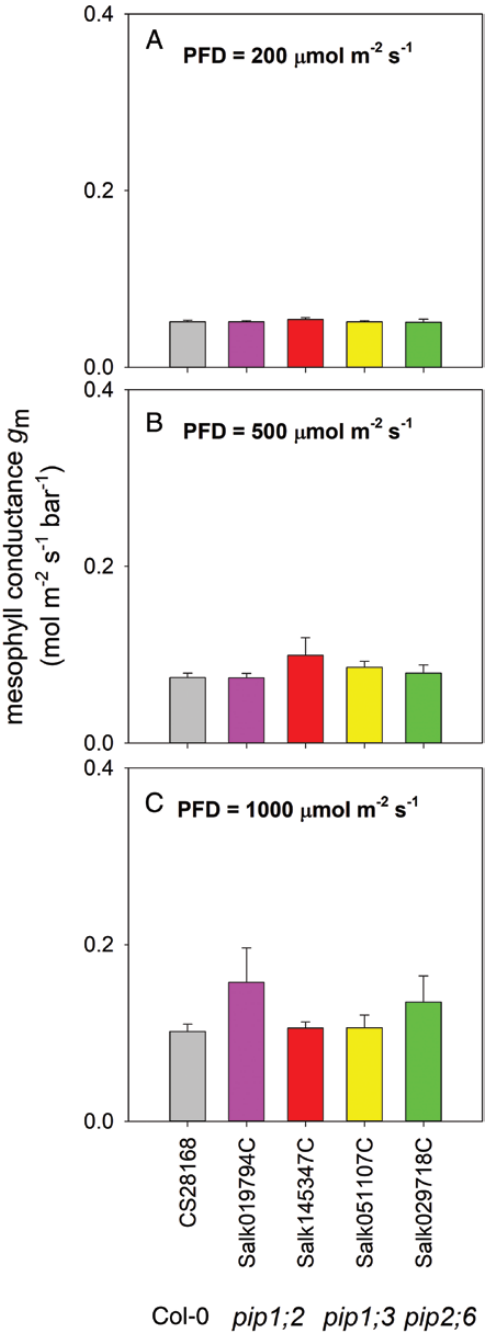

Fig. 2. Mesophyll conductance estimated from constant *J* in Arabidopsis *pip1;2*, *pip1;3*, and *pip2;6* mutants. (A) Mesophyll conductance g_m estimated by parallel gas exchange and chlorophyll fluorescence measurements, using constant *J* method at light intensity of 200 µmol m^{-2} s^{-1} in *pip1;2*, *pip1;3*, and *pip2;6* T-DNA insertional mutants and Col-0 control. Bars and error bars show means ±SE (n=9–11). (B) As (A) but at light intensity of 500 µmol m^{-2} s^{-1}. (C) As (A) but at light intensity of 1000 µmol m^{-2} s^{-1}.

g_m estimated from variable J

Unlike the constant *J* method, the variable *J* method does not depend on *J* and g_m to be invariant with changes in CO_2 concentration, but instead can be used to estimate g_m under a range of measurement conditions, provided photorespiration is not suppressed to insignificant rates. The variable *J* method was first used to assess the light response of g_m. In contrast to the significant light effect on g_m found with the constant *J* method, g_m was relatively constant for PFD above 200 µmol m^{-2} s^{-1} averaging 0.12 mol m^{-2} s^{-1} bar^{-1}. Somewhat erratic variations in g_m at lower PFD were observed, probably due to limited signal to noise to resolve g_m at these low light intensities. Bootstrapping-derived 95% confidence intervals around the mean of g_m for each genotype were clearly overlapping between both *pip1-2*

mutants, as well as for *pip1-3*, *pip2-6*, and Col-0 at all light levels (Fig. 3) and the same was true for stomatal conductance, measured in parallel (see Supplementary Fig. S2). Hence, consistent with the $\Delta^{13}C$ and constant *J* methods, the absence of PIP1-2, PIP1-3, and PIP2-6 seemed to have no significant effect on g_m at varying light levels.

The variable *J* method was also used to estimate g_m under ambient and subambient CO_2 concentrations at 1000 µmol m^{-2} s^{-1} PFD. At 400 µmol mol^{-1}, average g_m estimates were similar to those from the constant *J* estimates at 1000 µmol m^{-2} s^{-1} PFD (averaging 0.12 mol m^{-2} s^{-1} bar^{-1}, Fig. 4). Estimates of g_m were not significantly affected by CO_2 concentration, although the confidence intervals widened somewhat towards the lowest CO_2 concentration. Once again, 95% confidence intervals for g_m entirely overlapped across all measured conditions between the mutants and Col-0 (Fig. 4).

CO_2 compensation point C_i^*

Another way to assess differences in g_m is by determination of the CO_2 compensation point in the absence of dark respiration. The CO_2 compensation point reflects the CO_2 partial pressure where CO_2 uptake via RuBP carboxylation equals CO_2 release via photorespiration. Within the chloroplast, the CO_2 compensation point (in this case named Γ^*) is primarily determined by the specificity of Rubisco. However, when the CO_2 compensation point is measured on the basis of intercellular airspace CO_2 concentration (i.e. C_i^*), the level becomes dependent on the gradient of CO_2 partial pressure between chloroplast stroma and airspace, which is affected by the diffusion conductance g_m. C_i^* values ranged from 36.1 to 39.7 µbar, and did not show a significant effect of genotype (Fig. 5, P=0.52). Also indicated in Fig. 5 is the value of Γ^* at 24 °C, which was the average leaf temperature during the C_i^* determinations. Interestingly, all of the measured C_i^* values were equal to or higher than Γ^* (P>0.22), which may reflect a modest contribution of the chloroplast envelope to the overall diffusion resistance.

Photosynthetic capacity and efficiency

The response of A_n to light and CO_2 was also analysed for potential effects of the aquaporin deficiencies on photosynthetic capacity and efficiency. A_n increased steadily with absorbed

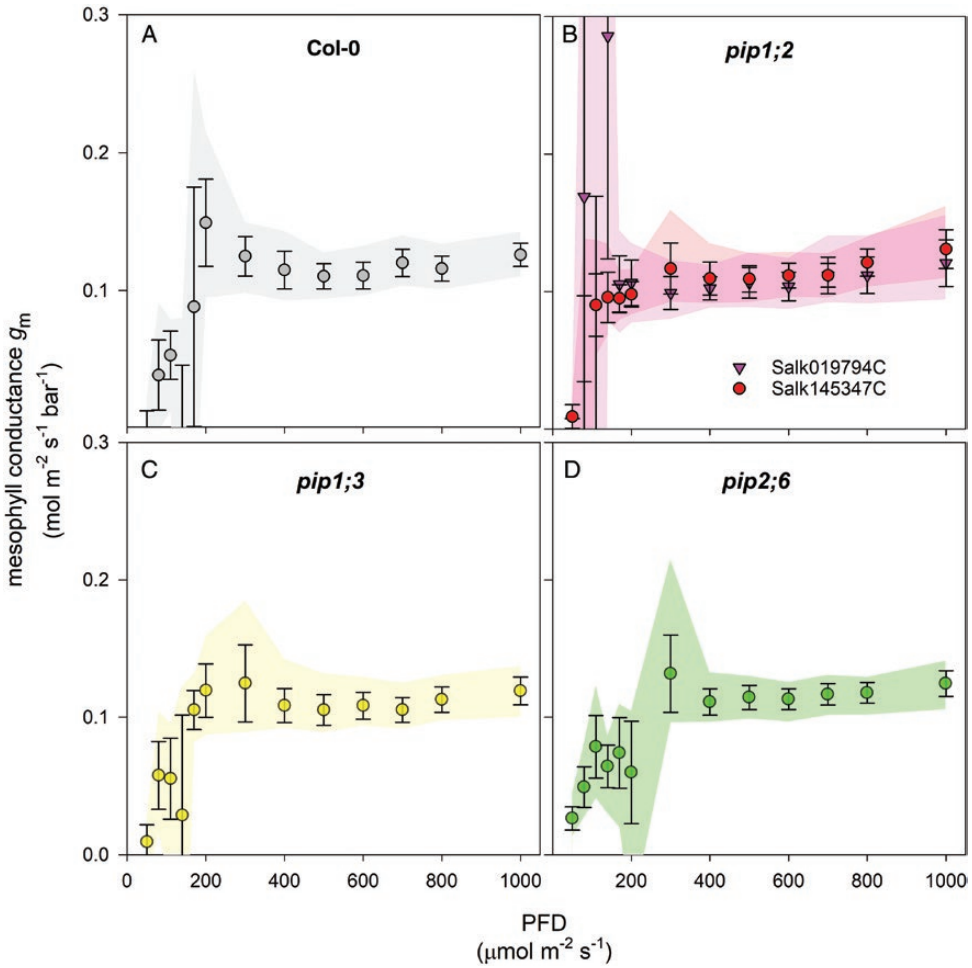

Fig. 3. Mesophyll conductance estimated from variable *J* as a function of PFD in Arabidopsis *pip1;2*, *pip1;3*, and *pip2;6* mutants. Mesophyll conductance (g_m) estimated by parallel gas exchange and chlorophyll fluorescence measurements across a light response curve, using variable *J* method. Estimates for g_m are depicted as a function of absorbed light intensity (PFD) for (A) Col-0 control plants, (B) *pip1;2* mutant plants from Salk019794C and Salk145347C, (C) *pip1;3* mutant plants, and (D) *pip2;6* mutant plants. Symbols and error bars show means ±SE (n=8). Shaded areas indicate 95% confidence intervals.

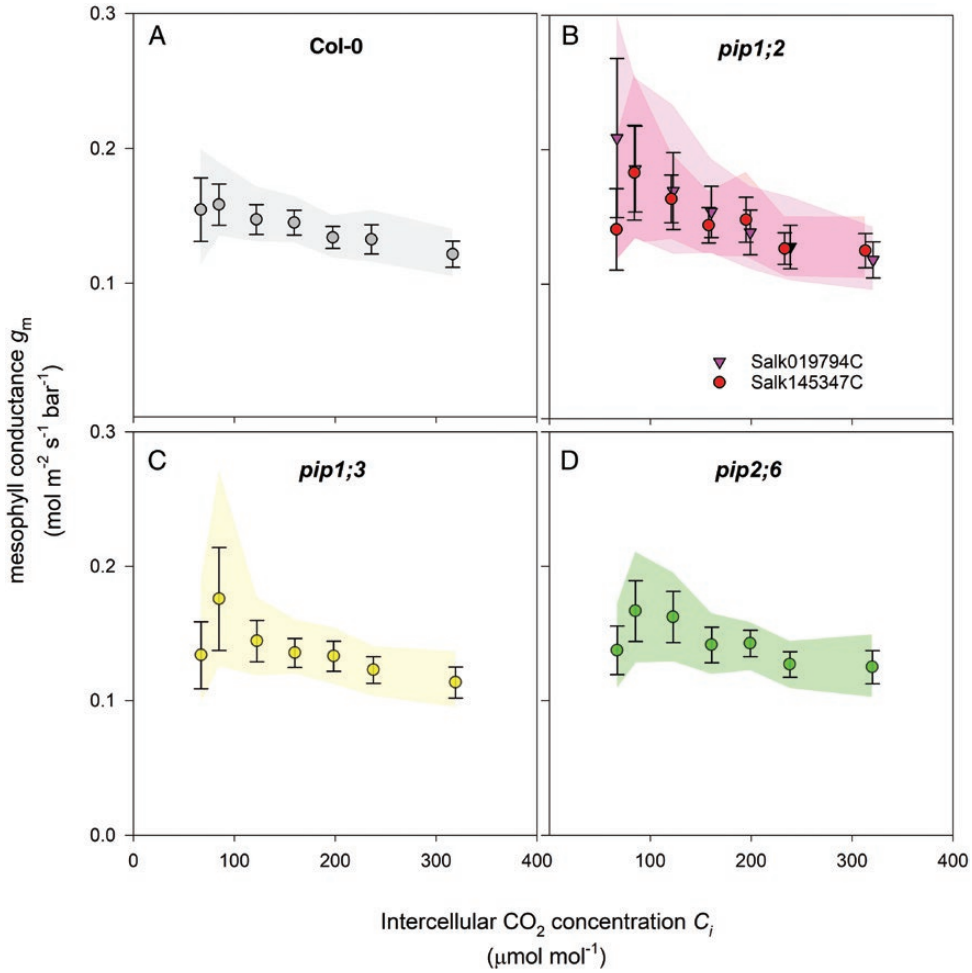

Fig. 4. Mesophyll conductance estimated from variable *J* as a function of CO_2 in Arabidopsis *pip1;2*, *pip1;3*, and *pip2;6* mutants. Mesophyll conductance (g_m) estimated by parallel gas exchange and chlorophyll fluorescence measurements across a CO_2 response curve, using variable *J* method. Estimates for g_m are depicted as a function of CO_2 concentration in the substomatal cavity (C_i) for (A) Col-0 control plants, (B) *pip1;2* mutant plants from Salk019794C and Salk145347C, (C) *pip1;3* mutant plants, and (D) *pip2;6* mutant plants. Symbols and error bars show means ±SE (*n*=8). Shaded areas indicate 95% confidence intervals.

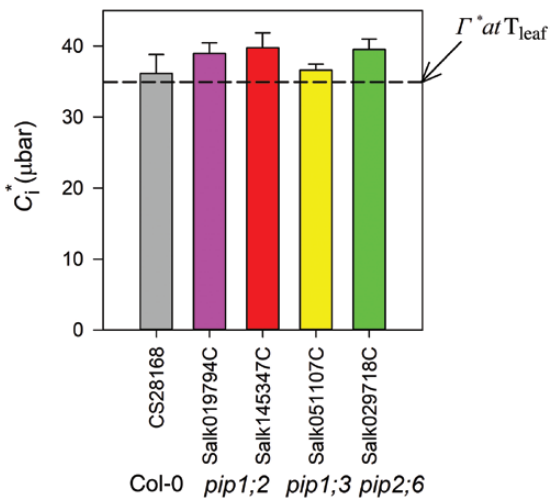

Fig. 5. Photosynthetic CO_2 compensation point (C_i^*) in Arabidopsis *pip1;2*, *pip1;3*, and *pip2;6* mutants. The CO_2 compensation point (C_i^*) was estimated using the slope–intercept method (Walker and Ort, 2015) from measurements of A_n and C_i at five subambient CO_2 concentrations across five light intensities for each leaf. Bars show means ±SE (*n*=3). Also indicated is the CO_2 compensation point Γ^* on a chloroplastic CO_2 basis (35 µbar), at the average leaf temperature during the measurements (24.0±0.1 °C).

PFD until an inflection point around 250 µmol m^{-2} s^{-1} (Fig. 6A–D), above which only marginal further increases were registered. Average A_n at the highest PFD was very similar between the aquaporin mutants and the Col-0 control, ranging from 13.3 to 13.6 µmol m^{-2} s^{-1}. Initial slopes derived from the first four points at low light also did not vary between genotypes (P=0.97), averaging between 0.056 and 0.058 mol CO_2 mol^{-1} absorbed photons (Table 1). Corresponding light responses of whole-chain electron transport rate derived from chlorophyll fluorescence measurements were used to derive J_{max}, which ranged between 90.7 and 92.7 µmol m^{-2} s^{-1} and was very similar between genotypes (Table 1). Responses of A_n to CO_2 concentration in intercellular airspaces (C_i) were also measured (Fig. 6E–H). A_n increased steeply up to the operating point around 300 µmol mol^{-1} above which further increases were less pronounced and A_n eventually reached a plateau ranging between 16.7 and 17.2 µmol m^{-2} s^{-1}. Clearly, 95% confidence intervals show great overlap between all genotypes. In addition, $V_{c,max}$ values on a C_c basis were derived from fitting a biochemical photosynthesis model on the CO_2 responses, using average g_m values from the variable *J* results at high light to convert from C_i to C_c. As could be expected from the lack

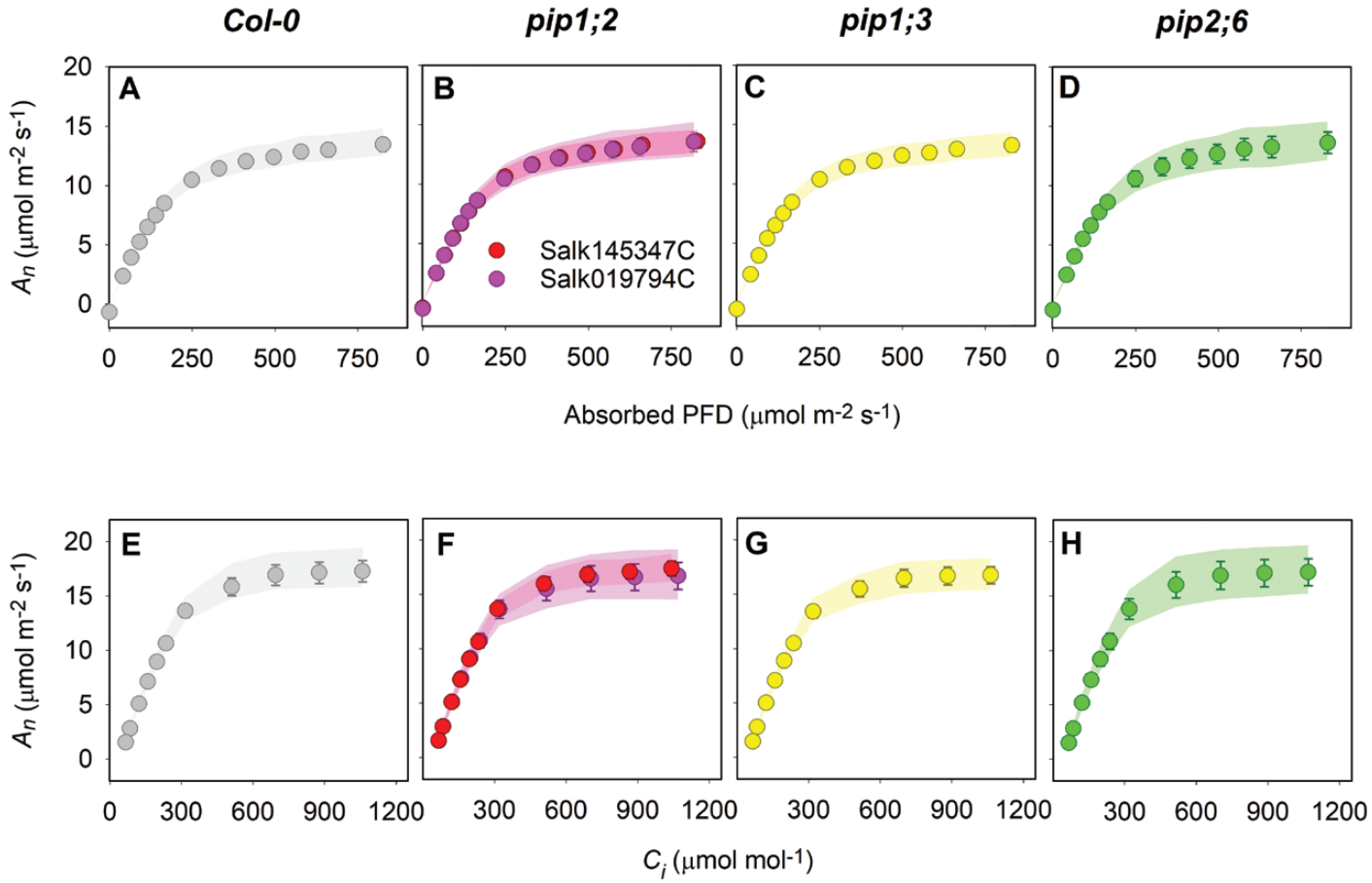

Fig. 6. Light and CO_2 response of net CO_2 assimilation in Arabidopsis *pip1;2*, *pip1;3*, and *pip2;6* mutants. Net assimilation rate is shown as a function of absorbed light intensity (A–D) or CO_2 concentration in the substomatal cavity (C_i; E–H) for Col-0 control plants (A, E), *pip1;2* mutant plants from Salk19794C and Salk145347C (B, F), *pip1;3* mutant plants (C, G), and *pip2;6* mutant plants (D, H). Symbols and error bars show means ±SE (n=8). Shaded areas indicate 95% confidence intervals.

Table 1. Photosynthetic parameters of Arabidopsis ecotype Col-0 (CS28168) and mutants deficient in PIP1;2 (Salk019794C and Salk145347C), PIP1;3 (Salk051107C) and PIP2;6 (Salk029718C) derived from responses of net assimilation rate (A_n) and whole-chain electron transport rate (J) to light intensity (PFD) and CO_2 concentration

Genotype	Mutated locus	Initial slope A_n/PFD (n.s., P=0.97)	A_{sat} (n.s., P=0.96)	J_{max} (n.s., P=0.99)	$V_{c,max}$ (n.s., P=0.98)
CS28168	n.a.	0.056±0.002	15.1±0.7	92.2±3.3	76.6±6.2
Salk019794C	PIP1;2	0.058±0.003	15.5±1.0	90.7±5.1	79.7±9.6
Salk145347C	PIP1;2	0.057±0.002	15.0±0.5	90.8±4.6	75.0±3.5
Salk051107C	PIP1;3	0.056±0.002	15.0±0.5	92.7±4.9	77.1±6.2
Salk29718C	PIP2;6	0.057±0.002	15.6±0.9	90.7±3.2	81.0±9.9

Values are shown as means ±SE (n=8 biological replicates). P-values indicate significance of analysis of variance. n.a., not applicable; n.s., not significant.

of variation between genotypes in the A_n/C_i responses as well as g_m estimates, $V_{c,max}$ also did not vary significantly between genotypes, ranging between 75.0 and 81.0 μmol m^{-2} s^{-1}.

Finally, to rule out any differences in CO_2 supply in the chloroplast, the operating efficiency of whole-chain electron transfer through PSII (Φ_{PSII}) from the light response curves was plotted against the quantum yield of CO_2 fixation, obtained by dividing the gross assimilation rate (A_n+R_d) by absorbed PFD (Fig. 7). Symbols for the different genotypes overlapped for all light intensities and were very similar at high light, indicating that the relationship between electron transfer and CO_2 fixation had not been altered in the *pip* mutant lines.

Discussion

CO_2 assimilation in C_3 species under atmospheric conditions is typically limited by the diffusion conductance to CO_2 transfer from atmosphere to chloroplast stroma. Part of this limitation resides in the pathway from intercellular airspace to

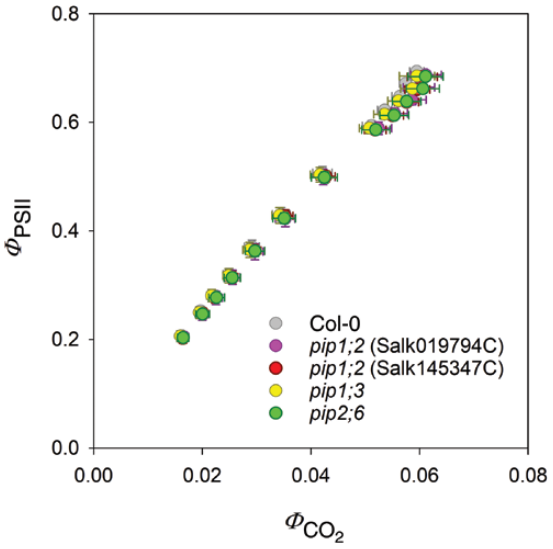

Fig. 7. Quantum yield of photosystem II as a function of quantum yield of CO_2 fixation in Arabidopsis *pip1;2*, *pip1;3*, and *pip2;6* mutants. Gas exchange data from the light response curves shown in Fig. 6 were used to compute the quantum yield of CO_2 fixation (Φ_{CO_2}). Quantum yield for whole-chain electron transfer through photosystem II (Φ_{PSII}) was estimated from parallel chlorophyll fluorescence measurements. Symbols and error bars show means ±SE (n=8). Symbol colours depict specific PIP mutants or Col-0 control as indicated in key.

chloroplast stroma and improving the CO_2 transfer conductance across this pathway (g_m) holds promise to increase both photosynthesis and intrinsic water use efficiency. Based on previous work, CO_2-conducting aquaporins may have a role in facilitation of CO_2 transfer across membranes, which has been suggested to improve g_m and A_n. Here, we explored the role of three different aquaporins on g_m in T-DNA insertional mutants using four different methods, but failed to establish any significant phenotypic difference from the Col-0 background. Methods to estimate g_m are indirect and all have their limitations (Pons *et al.*, 2009). Therefore, the most effective way of assessing g_m is to use multiple methods as demonstrated here. Critically, all methods demonstrated convincingly that g_m and photosynthetic efficiency were unaffected between the three aquaporin knock-outs and wild-type. Here these findings are first discussed for *PIP1;3* and *PIP2;6* and subsequently for *PIP1;2*.

g_m and photosynthetic efficiency in pip1;3 and pip2;6

PIP1;3 and *PIP2;6* have not previously been investigated for a role in g_m and photosynthetic efficiency. Here, they were selected to be included in our study based on sequence similarity with *PIP1;2* (*PIP1;3*), co-expression with photosynthetic gene expression (*PIP2;6*), significant expression in leaves (both *PIP1;3* and *PIP2;6*) and presence of a conserved sequence on the E-loop (Mori *et al.*, 2014), which may facilitate CO_2 conductance (both *PIP1;3* and *PIP2;6*). However, based on our results, none of these attributes appeared predictive for effects on either g_m or photosynthetic efficiency. Instead, our null hypothesis (no effect of T-DNA-insertion mutation on g_m and photosynthetic efficiency) was convincingly confirmed for all measurements. The values of g_m varied somewhat between the estimation method applied, with the isotope discrimination method yielding slightly higher estimates (0.19–0.24 mol m^{-2} s^{-1} bar^{-1}) than the fluorescence-based methods (0.12–0.13 mol m^{-2} s^{-1} bar^{-1}). Both compare well with previous estimates of g_m in Col-0 of 0.16 mol m^{-2} s^{-1} bar^{-1} using the variable J method (Heckwolf *et al.*, 2011) or 0.22 mol m^{-2} s^{-1} bar^{-1} using the carbon isotope method (Von Caemmerer and Evans, 2015). Use of several methods should protect the conclusions against the considerable uncertainty associated with assumed values of specific fractionation factors (isotope method), potential differences between chloroplast populations sampled by fluorescence versus gas exchange (fluorescence methods) and further artefactual responses of g_m to measurement conditions. With regard to the uncertain contribution of the chloroplast envelope to g_m, our C_i* estimates were higher than Γ*, which would be consistent with a significant contribution of the chloroplast envelope resistance relative to the resistance of plasma membrane and cell wall resistance to CO_2 transfer (Walker and Ort, 2015). However, it should be kept in mind that these differences are within the uncertainty range of the infra-red gas analyser calibration and cross-comparison between different studies and instruments may therefore also reflect small calibration differences.

g_m and photosynthetic efficiency in pip1;2

Whereas the lack of evidence for a role of *PIP1;3* or *PIP2;6* in diffusion limitation of photosynthesis may have been expected, the two mutant lines for *pip1;2* (Salk145347C and Salk019794C), which were intended to be our positive control, also failed to show a decrease in g_m and photosynthetic efficiency in contrast to previous reports (Heckwolf *et al.*, 2011; Uehlein *et al.*, 2012). These surprising results are discussed below in the context of (i) functional redundancy between aquaporin family members and (ii) role of hydraulic conductance.

Functional redundancy

The Arabidopsis genome includes five PIP1 and six PIP2 isoforms (Quigley *et al.*, 2002). Several specific isoforms have been implicated in functional roles, divergent from cellular water conductance. For example, *PIP1;4* was shown to be involved in H_2O_2 signalling in response to bacterial pathogens (Tian *et al.*, 2016) and *PIP2;1* regulates activity of guard cell anion channel SLAC1 via interaction with βCA4 (Wang *et al.*, 2016) and is also involved in ABA- or pathogen-induced stomatal closure via facilitated transfer of H_2O_2 into guard cells (Rodrigues *et al.*, 2017). However, despite this functional diversification, considerable functional redundancy may remain, which would allow compensation between different aquaporin isoforms to mask effects of single gene knock-outs. It has been reported that no up-regulation of other PIP isoforms could be detected in *pip1;2* mutants, relative to the wild-type background (Postaire *et al.*, 2010; Boursiac *et al.*, 2005). However, without a complete understanding of the role of *PIP1;2* in g_m (if any), we cannot rule out that the effects of knock-out

mutation of *PIP1;2* might have been compensated by functionally overlapping isoforms.

Effects of hydraulic conductance and light intensity during growth

Whereas substantial functional diversification of PIPs has been observed, the water-conducing function of the pore is often conserved. To interpret a physiological role of PIPs in g_m, a parallel facilitating effect on membrane conductance to water has the potential to confound analyses. In experimental membrane systems, *PIP1;2* expression improved membrane water conductance of *Xenopus laevis* oocytes (Kammerloher *et al.*, 1994) but not of yeast protoplasts (Heckwolf *et al.*, 2011). In Arabidopsis protoplasts, antisense silencing of *PIP1;2* (Kaldenhoff *et al.*, 1998) or T-DNA insertional mutagenesis (Postaire *et al.*, 2010) reduced membrane water conductance more than 2-fold. The latter results are arguably most relevant for the role of PIP1;2 *in planta* and are backed up by results at the whole-plant level, where hydraulic conductance of whole Arabidopsis rosettes was significantly reduced by knock-out mutation of *PIP1;2* (Postaire *et al.*, 2010; Prado *et al.*, 2013). A role in hydraulic conductance at the plant level is also consistent with the high expression levels of *PIP1;2* in roots, where it can contribute up to 30% to hydrostatic water transport (Postaire *et al.*, 2010). One emerging aspect to consider here is the intricate network of interactions between PIP1 and PIP2 family members (Yaneff *et al.*, 2015). For example, several PIP1s require co-expression with PIP2 isoforms to localize to the plasma membrane, and the formation of specific heterotetramers between PIP1 and PIP2 isoforms seems to be important for conductivity of the pore (Otto *et al.*, 2010). Yaneff *et al.* (2015) suggested that it may be necessary to consider pairs of PIP1s and PIP2s. Consistent with these suggestions, the interactomes of Arabidopsis PIP1;2 and PIP2;1 were found to overlap by 80% (Bellati *et al.*, 2016), which may be explained by complex formation between the two PIP isoforms. As a consequence of this work, it is quite likely that PIP1;2 may also affect hydraulic conductance indirectly, due to interactions with the PIP2 isoforms, which are generally recognized as stronger water conductors than PIP1s.

Leaf hydraulic conductivity is an important determinant of photosynthetic capacity (Scoffoni *et al.*, 2016) and hydraulic conductivity and g_m may also be loosely coordinated (Flexas *et al.*, 2013*b*). As a result, if previous findings for altered g_m and A_n by Heckwolf *et al.* (2011) were not direct effects of altered membrane conductance to CO_2, but rather more indirect effects resulting from alterations in plant hydraulic conductivity, this may provide a clue to the lack of repeatability of the phenotype in our hands. In this context, the difference in growing conditions between studies may be important. In the current paper, plants were grown at 200 μmol m^{-2} s^{-1} in controlled environment growth chambers, which was continuously monitored and regulated via an automated feedback loop and a PFD sensor at plant level. Much lower growing light intensity of 100 μmol m^{-2} s^{-1} (Uehlein *et al.*, 2012) or 70–80 μmol m^{-2} s^{-1} (Heckwolf *et al.*, 2011) was used for the reports in which g_m appeared to be affected by the absence of *PIP1;2*. The light regime during growth was shown to have a substantial effect on aquaporin expression (Postaire *et al.*, 2010), and leaf hydraulic conductance measurements on plants grown at 120 μmol m^{-2} s^{-1} (Levin *et al.*, 2007) were substantially lower than for plants grown at 200–250 μmol m^{-2} s^{-1} (Martre *et al.*, 2002; Postaire *et al.*, 2010). We should emphasize here, that in addition to photosynthetic parameters and g_m, stomatal conductance g_s was also very similar between mutant plants and control (see Supplementary Fig. S2). Thus, if we assume that the co-variation between hydraulic conductance and g_m implies some level of mechanistic coordination (Flexas *et al.*, 2018), we may speculate that the higher light conditions during growth of our plants could have raised hydraulic conductance in both Col-0 and mutant plants sufficiently to remove any observable effects on g_s and g_m such as observed previously.

Implications for the role of aquaporins in g_m and photosynthetic efficiency

Based on previous data (Heckwolf *et al.*, 2011; Uehlein *et al.*, 2012), Arabidopsis mutants deficient in AtPIP1;2 may clearly show a photosynthetic phenotype. However, our data demonstrate that this phenotype is not universally observed, and may only manifest under a specific set of growth conditions. Curiously, previous reports of photosynthetic depression in *pip1;2* mutants in Arabidopsis (Heckwolf *et al.*, 2011; Uehlein *et al.*, 2012) and tobacco *aqp1* mutants (Flexas *et al.*, 2006) seem to indicate a more severe difference in A_n at high CO_2 concentrations. This appears at odds with an increased diffusive limitation of photosynthesis, since CO_2 saturation should remove, rather than aggravate, the limitation of A_n by CO_2. Two hypotheses could be formulated based on this apparent discrepancy. First, cause and effect may have been swapped in previous interpretation of this phenotype. Namely, in the aforementioned studies, photosynthetic efficiency may have responded to these specific aquaporin deficiencies via a mechanism independent of g_m. In light of several recent findings of PIPs in H_2O_2 signal transduction (Tian *et al.*, 2016; Rodrigues *et al.*, 2017), we speculate that Arabidopsis PIP1;2 might also have a role in ROS signalling cascades, either directly or in conjunction with PIP2;1, which can have a profound effect on photosynthetic gene expression (Gorecka *et al.*, 2014; Exposito-Rodriguez *et al.*, 2017). If so, decreased g_m may result pleiotropically from effects on photosynthetic capacity and A_n rather than being directly affected by the absence of PIP1;2. This hypothesis would be consistent with the similarity between the transcriptome of *pip1;2* mutant plants and plants grown at CO_2 starvation as observed by Boudichevskaia *et al.* (2015), without requiring a direct CO_2 supplementation effect of *PIP1;2* on photosynthesis. Alternatively, if specific aquaporin deficiencies reduce the chloroplastic CO_2 concentration, the increased Rubisco limitation of A_n may have led to down-regulation of superfluous RuBP regeneration capacity at supra-ambient CO_2 concentrations. However, substantial acclimation potential is typically observed with photosynthetic capacity, and one might then have expected Rubisco content or activation state to be up-regulated in parallel. Of course, these suggestions are all necessarily speculative in the absence

of an observable phenotype of the PIP mutants described here. Further explorations of the role of PIPs in photosynthetic efficiency should verify these hypotheses. In addition, in light of our results, future work will need to focus on the manifestation of a g_m or A_n phenotype as a function of the conditions during plant cultivation, in particular light intensity. However, in the context of increasing photosynthetic efficiency, our results suggest that our current understanding of the physiological role of PIPs in CO_2 transfer across membranes may need to be revised.

Supplementary data

Supplementary data are available at *JXB* online.

Fig. S1. Molecular verification of *pip1;2*, *pip1;3*, and *pip2;6* T-DNA insertional mutants.

Fig. S2. Stomatal conductance to water vapour as a function of absorbed light intensity in Col-0 control and *pip1;2*, *pip1;3* and *pip2;6* T-DNA insertional mutants.

Table S1. Primer sequences for PCR, RT-PCR, and RT-qPCR.

Acknowledgements

We would like to thank Katherine Kucera for assistance in plant propagation and confirmation of the molecular phenotype. This work was supported by the research project Realizing Increased Photosynthetic Efficiency (RIPE) funded by the Bill & Melinda Gates Foundation, Foundation for Food and Agriculture Research, and the Department for International Development under grant number OPP1172157.

References

Agre P, Sasaki S, Chrispeels MJ. 1993. Aquaporins: a family of water channel proteins. The American Journal of Physiology **265**, F461.

Ainsworth EA, Long SP. 2005. What have we learned from 15 years of free-air CO_2 enrichment (FACE)? A meta-analytic review of the responses of photosynthesis, canopy properties and plant production to rising CO_2. New Phytologist **165**, 351–371.

Alonso JM, Stepanova AN, Leisse TJ *et al*. 2003. Genome-wide insertional mutagenesis of *Arabidopsis thaliana*. Science **301**, 653–657.

Alexandersson E, Fraysse L, Sjövall-Larsen S, Gustavsson S, Fellert M, Karlsson M, Johanson U, Kjellbom P. 2005. Whole gene family expression and drought stress regulation of aquaporins. Plant Molecular Biology **59**, 469–484.

Bansal A, Sankararamakrishnan R. 2007. Homology modeling of major intrinsic proteins in rice, maize and *Arabidopsis*: comparative analysis of transmembrane helix association and aromatic/arginine selectivity filters. BMC Structural Biology **7**, 27.

Bellati J, Champeyroux C, Hem S, Rofidal V, Krouk G, Maurel C, Santoni V. 2016. Novel aquaporin regulatory mechanisms revealed by interactomics. Molecular & Cellular Proteomics **15**, 3473–3487.

Boudichevskaia A, Heckwolf M, Kaldenhoff R. 2015. T-DNA insertion in aquaporin gene AtPIP1;2 generates transcription profiles reminiscent of a low CO_2 response. Plant, Cell & Environment **38**, 2286–2298.

Boursiac Y, Chen S, Luu DT, Sorieul M, van den Dries N, Maurel C. 2005. Early effects of salinity on water transport in Arabidopsis roots. Molecular and cellular features of aquaporin expression. Plant Physiology **139**, 790–805.

Da Ines O. 2008. Functional analysis of PIP2 aquaporins in *Arabidopsis thaliana*. PhD Thesis, Ludwig-Maximilians-Universität München.

Endeward V, Al-Samir S, Itel F, Gros G. 2014. How does carbon dioxide permeate cell membranes? A discussion of concepts, results and methods. Frontiers in Physiology **4**, 382.

Evans JR, Kaldenhoff R, Genty B, Terashima I. 2009. Resistances along the CO_2 diffusion pathway inside leaves. Journal of Experimental Botany **60**, 2235–2248.

Evans JR, Sharkey TD, Berry JA, Farquhar GD. 1986. Carbon isotope discrimination measured concurrently with gas exchange to investigate CO_2 diffusion in leaves of higher plants. Australian Journal Plant Physiology **13**, 281–292.

Evans JR, von Caemmerer S. 2013. Temperature response of carbon isotope discrimination and mesophyll conductance in tobacco. Plant, Cell & Environment **36**, 745–756.

Exposito-Rodriguez M, Laissue PP, Yvon-Durocher G, Smirnoff N, Mullineaux PM. 2017. Photosynthesis-dependent H_2O_2 transfer from chloroplasts to nuclei provides a high-light signalling mechanism. Nature Communications **8**, 49.

FAO, IFAD, UNICEF, WFP and WHO. 2017. The state of food security and nutrition in the world 2017. Building resilience for peace and food security. Rome: FAO.

Flexas J, Carriquí M, Nadal M. 2018. Gas exchange and hydraulics during drought in crops: who drives whom? Journal of Experimental Botany **69**, 3791–3795.

Flexas J, Niinemets U, Gallé A, *et al*. 2013*a*. Diffusional conductances to CO_2 as a target for increasing photosynthesis and photosynthetic water-use efficiency. Photosynthesis Research **117**, 45–59.

Flexas J, Ribas-Carbó M, Hanson DT, Bota J, Otto B, Cifre J, McDowell N, Medrano H, Kaldenhoff R. 2006. Tobacco aquaporin NtAQP1 is involved in mesophyll conductance to CO_2 *in vivo*. The Plant Journal **48**, 427–439.

Flexas J, Scoffoni C, Gago J, Sack L. 2013*b*. Leaf mesophyll conductance and leaf hydraulic conductance: an introduction to their measurement and coordination. Journal of Experimental Botany **64**, 3965–3981.

Frick A, Järvå M, Törnroth-Horsefield S. 2013. Structural basis for pH gating of plant aquaporins. FEBS Letters **587**, 989–993.

Genty B, Briantais J-M, Baker NR. 1989. The relationship between the quantum yield of photosynthetic electron transport and quenching of chlorophyll fluorescence. Biochimica et Biophysica Acta **990**, 87–92.

Gorecka M, Alvarez-Fernandez R, Slattery K, McAusland L, Davey PA, Karpinski S, Lawson T, Mullineaux PM. 2014. Abscisic acid signalling determines susceptibility of bundle sheath cells to photoinhibition in high light-exposed *Arabidopsis* leaves. Philosophical Transactions of the Royal Society of London. Series B, Biological Sciences **369**, 20130234.

Groszmann M, Osborn HL, Evans JR. 2017. Carbon dioxide and water transport through plant aquaporins. Plant, Cell & Environment **40**, 938–961.

Gu L, Sun Y. 2014. Artefactual responses of mesophyll conductance to CO_2 and irradiance estimated with the variable *J* and online isotope discrimination methods. Plant, Cell & Environment **37**, 1231–1249.

Harley PC, Loreto F, Di Marco G, Sharkey TD. 1992. Theoretical considerations when estimating the mesophyll conductance to CO_2 flux by analysis of the response of photosynthesis to CO_2. Plant Physiology **98**, 1429–1436.

Hasegawa T, Sakai H, Tokida T, *et al*. 2013. Rice cultivar responses to elevated CO_2 at two free-air CO_2 enrichment (FACE) sites in Japan. Functional Plant Biology **40**, 148–159.

Heckwolf M, Pater D, Hanson DT, Kaldenhoff R. 2011. The *Arabidopsis thaliana* aquaporin AtPIP1;2 is a physiologically relevant CO_2 transport facilitator. The Plant Journal **67**, 795–804.

Hunter MC, Smith RG, Schipanski ME, Atwood LW, Mortensen DA. 2017. Agriculture in 2050: recalibrating targets for sustainable intensification. BioScience **67**, 386–391.

Kaldenhoff R, Grote K, Zhu JJ, Zimmermann U. 1998. Significance of plasmalemma aquaporins for water-transport in *Arabidopsis thaliana*. The Plant Journal **14**, 121–128.

Kammerloher W, Fischer U, Piechottka GP, Schäffner AR. 1994. Water channels in the plant plasma membrane cloned by immunoselection from a mammalian expression system. The Plant Journal **6**, 187–199.

Köhler IH, Ruiz-Vera UM, VanLoocke A, Thomey ML, Clemente T, Long SP, Ort DR, Bernacchi CJ. 2017. Expression of cyanobacterial FBP/SBPase in soybean prevents yield depression under future climate conditions. Journal of Experimental Botany **68**, 715–726.

Kromdijk J, Głowacka K, Leonelli L, Gabilly ST, Iwai M, Niyogi KK, Long SP. 2016. Improving photosynthesis and crop productivity by accelerating recovery from photoprotection. Science **354**, 857–861.

Kromdijk J, Griffiths H, Schepers HE. 2010. Can the progressive increase of C_4 bundle sheath leakiness at low PFD be explained by incomplete suppression of photorespiration? Plant, Cell & Environment **33**, 1935–1948.

Levin M, Lemcoff JH, Cohen S, Kapulnik Y. 2007. Low air humidity increases leaf-specific hydraulic conductance of *Arabidopsis thaliana* (L.) Heynh (*Brassicaceae*). Journal of Experimental Botany **58**, 3711–3718.

Long SP, Marshall-Colon A, Zhu XG. 2015. Meeting the global food demand of the future by engineering crop photosynthesis and yield potential. Cell **161**, 56–66.

Loriaux SD, Avenson TJ, Welles JM, McDermitt DK, Eckles RD, Riensche B, Genty B. 2013. Closing in on maximum yield of chlorophyll fluorescence using a single multiphase flash of sub-saturating intensity. Plant, Cell & Environment **36**, 1755–1770.

Martre P, Morillon R, Barrieu F, North GB, Nobel PS, Chrispeels MJ. 2002. Plasma membrane aquaporins play a significant role during recovery from water deficit. Plant Physiology **130**, 2101–2110.

Maurel C. 1997. Aquaporins and water permeability of plant membranes. Annual Review of Plant Physiology and Plant Molecular Biology **48**, 399–429.

Maurel C, Boursiac Y, Luu DT, Santoni V, Shahzad Z, Verdoucq L. 2015. Aquaporins in plants. Physiological Reviews **95**, 1321–1358.

Mori IC, Rhee J, Shibasaka M, Sasano S, Kaneko T, Horie T, Katsuhara M. 2014. CO_2 transport by PIP2 aquaporins of barley. Plant & Cell Physiology **55**, 251–257.

Ort DR, Merchant SS, Alric J, *et al*. 2015. Redesigning photosynthesis to sustainably meet global food and bioenergy demand. Proceedings of the National Academy of Sciences, USA **112**, 8529–8536.

Otto B, Uehlein N, Sdorra S, *et al*. 2010. Aquaporin tetramer composition modifies the function of tobacco aquaporins. The Journal of Biological Chemistry **285**, 31253–31260.

Pons TL, Flexas J, von Caemmerer S, Evans JR, Genty B, Ribas-Carbo M, Brugnoli E. 2009. Estimating mesophyll conductance to CO_2: methodology, potential errors, and recommendations. Journal of Experimental Botany **60**, 2217–2234.

Postaire O, Tournaire-Roux C, Grondin A, Boursiac Y, Morillon R, Schaffner AR, Maurel C. 2010. A PIP1 aquaporin contributes to hydrostatic pressure-induced water transport in both the root and rosette of Arabidopsis. Plant Physiology **152**, 1418–1430.

Prado K, Boursiac Y, Tournaire-Roux C, Monneuse JM, Postaire O, Da Ines O, Schäffner AR, Hem S, Santoni V, Maurel C. 2013. Regulation of *Arabidopsis* leaf hydraulics involves light-dependent phosphorylation of aquaporins in veins. The Plant Cell **25**, 1029–1039.

Quigley F, Rosenberg JM, Shachar-Hill Y, Bohnert HJ. 2002. From genome to function: the *Arabidopsis* aquaporins. Genome Biology **3**, RESEARCH0001.

Ray DK, Mueller ND, West PC, Foley JA. 2013. Yield trends are insufficient to double global crop production by 2050. PLoS One **8**, e66428.

Rodrigues O, Reshetnyak G, Grondin A, Saijo Y, Leonhardt N, Maurel C, Verdoucq L. 2017. Aquaporins facilitate hydrogen peroxide entry into guard cells to mediate ABA- and pathogen-triggered stomatal closure. Proceedings of the National Academy of Sciences, USA **114**, 9200–9205.

Rosenthal DM, Locke AM, Khozaei M, Raines CA, Long SP, Ort DR. 2011. Over-expressing the C_3 photosynthesis cycle enzyme Sedoheptulose-1-7 Bisphosphatase improves photosynthetic carbon gain and yield under fully open air CO_2 fumigation (FACE). BMC Plant Biology **11**, 123.

Scoffoni C, Chatelet DS, Pasquet-Kok J, Rawls M, Donoghue MJ, Edwards EJ, Sack L. 2016. Hydraulic basis for the evolution of photosynthetic productivity. Nature Plants **2**, 16072.

South PF, Cavanagh AP, Liu HW, Ort DR. 2019. Synthetic glycolate metabolism pathways stimulate crop growth and productivity in the field. Science **363**, eaat9077.

Tholen D, Ethier G, Genty B, Pepin S, Zhu XG. 2012. Variable mesophyll conductance revisited: theoretical background and experimental implications. Plant, Cell & Environment **35**, 2087–2103.

Tian S, Wang X, Li P, Wang H, Ji H, Xie J, Qiu Q, Shen D, Dong H. 2016. Plant aquaporin AtPIP1;4 links apoplastic H_2O_2 induction to disease immunity pathways. Plant Physiology **171**, 1635–1650.

Tilman D, Balzer C, Hill J, Befort BL. 2011. Global food demand and the sustainable intensification of agriculture. Proceedings of the National Academy of Sciences, USA **108**, 20260–20264.

Törnroth-Horsefield S, Wang Y, Hedfalk K, Johanson U, Karlsson M, Tajkhorshid E, Neutze R, Kjellbom P. 2006. Structural mechanism of plant aquaporin gating. Nature **439**, 688–694.

Tournaire-Roux C, Sutka M, Javot H, Gout E, Gerbeau P, Luu DT, Bligny R, Maurel C. 2003. Cytosolic pH regulates root water transport during anoxic stress through gating of aquaporins. Nature **425**, 393–397.

Uehlein N, Lovisolo C, Siefritz F, Kaldenhoff R. 2003. The tobacco aquaporin NtAQP1 is a membrane CO_2 pore with physiological functions. Nature **425**, 734–737.

Uehlein N, Sperling H, Heckwolf M, Kaldenhoff R. 2012. The Arabidopsis aquaporin PIP1;2 rules cellular CO_2 uptake. Plant, Cell & Environment **35**, 1077–1083.

Von Caemmerer S. 2000. Biochemical models of leaf photosynthesis. Collingwood Australia: CSIRO Publishing.

Von Caemmerer S, Evans JR. 2015. Temperature responses of mesophyll conductance differ greatly between species. Plant, Cell & Environment **38**, 629–637.

Walker B, Ariza LS, Kaines S, Badger MR, Cousins AB. 2013. Temperature response of in vivo Rubisco kinetics and mesophyll conductance in *Arabidopsis thaliana*: comparisons to *Nicotiana tabacum*. Plant, Cell & Environment **36**, 2108–2119.

Walker BJ, Ort DR. 2015. Improved method for measuring the apparent CO_2 photocompensation point resolves the impact of multiple internal conductances to CO_2 to net gas exchange. Plant, Cell & Environment **38**, 2462–2474.

Wang C, Hu H, Qin X, Zeise B, Xu D, Rappel WJ, Boron WF, Schroeder JI. 2016. Reconstitution of CO_2 regulation of SLAC1 anion channel and function of CO_2-permeable PIP2;1 aquaporin as CARBONIC ANHYDRASE4 interactor. The Plant Cell **28**, 568–582.

Xu F, Wang K, Yuan W, *et al*. 2019. Overexpression of rice aquaporin OsPIP1;2 improves yield by enhancing mesophyll CO_2 conductance and phloem sucrose transport. Journal of Experimental Botany **70**, 671–681.

Yaneff A, Vitali V, Amodeo G. 2015. PIP1 aquaporins: Intrinsic water channels or PIP2 aquaporin modulators? FEBS Letters **589**, 3508–3515.